Journal of Applied Polymer Science

Capillary Study on Geometrical Dependence of Shear Viscosity of Polymer Melts

Xiang Lin,[1] Adrian Kelly,[2] Mike Woodhead,[2] Dongyun Ren,[1] Kuisheng Wang,[1] Phil Coates[2]

[1]College of Mechanical and Electrical Engineering, Beijing University of Chemical Technology, 100029 Beijing, China

[2]IRC in Polymer Engineering, School of Engineering, Design, and Technology, University of Bradford, Bradford, West Yorkshire, United Kingdom

Correspondence to: D. Ren (E-mail: dongyunr@163.com) or K. Wang (E-mail: kuishengw@163.com)

ABSTRACT: Geometrical dependence of viscosity of polymethylmethacrylate (PMMA) and high density polyethylene (HDPE) are studied by means of a twin-bore capillary rheometer based on power-law model. Contrary geometrical dependences of shear viscosity are observed for PMMA between 210 and 255°C, but similar geometrical dependences are revealed for HDPE between 190 and 260°C. The fact that wall slip can not successfully explain the irregular geometrical dependence of PMMA viscosity is found in this work. Then, pressure effect and dependence of fraction of free volume (FFV) on both pressure and temperature are proposed to be responsible for the geometrical dependence of capillary viscosity of polymers. The dependence of shear viscosity on applied pressure is first investigated based on the Barus equation. By introducing a shift factor, shear viscosity curves of PMMA measured under different pressures can be shifted onto a set of parallel plots by correcting the pressure effect and the less shear-thinning then disappears, especially at high pressure. Meanwhile, the FFV and combining strength among molecular chains are evaluated for both samples based on molecular dynamics simulation, which implies that the irregular geometrical dependence of PMMA viscosity can not be attributed to the wall slip behavior. © 2013 Wiley Periodicals, Inc. J. Appl. Polym. Sci. **2014**, *131*, 39982.

KEYWORDS: viscosity and viscoelasticity; rheology; properties and characterization

Received 7 July 2013; accepted 19 September 2013

DOI: 10.1002/app.39982

INTRODUCTION

Viscosity is the dominant factor affecting the flow ability of polymer melts during practical processing among all the rheological properties. High flow ability of melt is helpful to ease the flow resistance, especially for the flows in micron channel. Many scholars found that the flow behavior of polymer melts on the microscopic scale could be significantly different from that on the macroscopic scale.[1–12] The micro-shear viscosity, which was defined as the shear viscosity of polymeric melt flowing in micron channel, was found to deviate from the conventional shear viscosity measured on the macroscopic scale. Dependence of shear viscosity of molten polymers on die scale was found during capillary extrusion. Shear viscosity of polymers changed with the die scale in capillary flow was previously defined as geometrical dependence.[13] This geometrical dependence was mainly attributed to the wall-slip behavior in many literatures.[6–12,14–18] For example, Zhao et al.[14,15] suggested that the wall slip between polymer bulk and wall surface was largely contributed to the geometrical dependence of shear viscosity based on the entanglement-disentanglement slip mechanism for polymethylmethacrylate (PMMA) and adsorption-desorption slip mechanism for high density polyethylene (HDPE). The existence of a lubricating layer between the melt bulk and the wall surface was particularly considered as the main factor for the different geometrical dependence of viscosity of PMMA from that of HDPE. However, pressure sensitivity of viscosity was also reported as a dominant factor.[19–27] Effects of die scale and melt pressure on the slip velocity in microchannel were emphasized by Hatzikiriakos.[17]

Viscosity of polymer is well known to increase exponentially with pressure. The viscosity of branched polyethylene (PE) was found to be 14-fold of its value at atmospheric pressure when the pressure increased to 168 MPa by Maxwell and Jung[28] as early as 1957. Couch and Binding[25,29] and Fernádez et al.[30] suggested that the pressure effect is more important for those polymers with bulkier backbones: increasing pressure or decreasing temperature reduces the amount of free volume available to molecules, resulting in an increase in intermolecular interactions and thus in viscosity enhancement. Cardinaels et al.[31] discussed the constant shear rate pressure coefficient and the constant shear stress pressure coefficient through a superposition calculation, and a single shift factor was proposed to describe the

effect of both pressure and temperature simultaneously. Owing to the highly flexible chains of HDPE, it is much less sensitive to pressure than that of PMMA.[24,25,29,32] The pressure coefficient, which was derived from the Barus equation,[33] was usually used to quantify the pressure dependency of viscosity for polymers. Cardinaels et al.[31] pointed out that definitions of pressure coefficient mainly included shear rate-dependent,[32,34] shear rate-independent,[25,29,35] and temperature-dependent.[25,29,32,34,35] Depending on the method used or shear rate range under investigation, however, the values of pressure coefficient in these literatures present large variations, even for the same polymer. It is difficult to acquire accurate data of pressure coefficient with experimental process due to the inherent difficulty.

Often, geometrical dependence of viscosity mainly includes two modes: thickening and thinning. The former means that under the same strain rate the viscosity increases with the decrease of channel scale and the latter is quite the opposite. For instance, the polyolefins, such as PE and polypropylene (PP), present thinning geometrical dependence within the conventional range of shear rate during capillary extrusion; however, pronounced thickening phenomenon is well observed for PMMA and polystyrene (PS). In addition, shear thickening of polymers was also observed at ultra high strain rates after reaching the second quasi-Newtonian plateau through a particular apparatus.[22–24] Thus, pressure sensitivity of viscosity was emphasized for the deviation of capillary viscosity plots.[25,26] Compared with the polyolefins, capillary viscosity of PMMA melt showed a much stronger shear thickening effect at a relatively lower pressure. During capillary extrusion, high pressure is always coupled with high shear rate and thus pressure sensitivity of viscosity cannot be neglected any more. It should be noticed that shear thickening of PE melt was even observed at critical shear rate up to 1×10^7 s^{-1}, but this critical shear rate for PMMA was less than 1×10^6 s^{-1}. However, a strong sensitivity of zero shear viscosity to the molecular weight was also observed at very low shear rates due to the molecular weight-dependent free volume effect.[36]

This work mainly focuses on understanding the geometrical dependence of capillary viscosity of HDPE and PMMA through capillary measurements which was conducted by using three pairs of dies. Wall slip velocity calculated by the Mooney slip model was first estimated to explain this geometrical dependence of viscosity. Results showed that Mooney method can be used to evaluate slip velocity for HDPE but not fit to evaluate slip velocity for PMMA of which negative slip velocity was shown at low temperature. Then, the pressure sensitivity of viscosity was emphasized for the irregular viscosity dependence on the die scale, especially for PMMA. A shift factor, derived from the Barus equation, was adopted to correct the pressure effect for the PMMA shear viscosity. In addition, the combining force between molecular chains and fraction of free volume (FFV) were finally considered for further understanding the geometrical dependency of viscosity.

EXPERIMENTAL

Twin-Bore Capillary Rheometer

A twin-bore capillary rheometer RH10 (BOHLIN INSTRUMENTS, UK) was adopted and capillary dies of D = 0.25, 0.50, and 1.00 mm with the same aspect ratio of 16 were used. Additional orifice die of effectively zero length (ratio of L/D is less than 0.25) is fitted with each capillary die for directly measuring the entrance pressure drop. This capillary rheometer is running by piston compression at several discrete stages. Apparent shear rate $\dot{\gamma}_{app}$ (s^{-1}) and the shear stress τ_w (Pa) are given as[37,38]:

$$\dot{\gamma}_{app} = \frac{4Q}{\pi R^3}, \tag{1}$$

$$\tau_w = \frac{R\Delta P}{2L}. \tag{2}$$

The apparent shear rate is not the true shear rate $\dot{\gamma}_w$ (s^{-1}) at the wall surface and is generally corrected with the Rabinowitsch correction for non-Newtonian liquids:

$$\dot{\gamma}_w = \frac{4Q}{\pi R^3}\left(\frac{3n+1}{4n}\right). \tag{3}$$

Then, the shear viscosity η_s (Pa·s) can be calculated by power-law model as

$$\eta_s = \frac{\tau_w}{\dot{\gamma}_w}. \tag{4}$$

In eqs. (1)–(4), n is the non-Newtonian index, R is the radius (m) of the capillary having a length of L (m), and Q is the volumetric flow rate (m^3/s) through the capillary under a pressure drop ΔP (Pa) between the entrance and exit along the capillary.

Materials

A PMMA grade VH067A (Mitsubishi Rayon, Japan) with a weight average molecular weight of 92,000, a molecular weight distribution of 1.937 and a density of about 1.20 g/cm^3 was adopted. This PMMA is a linear polymer with short branching. The second polymer is commercially available HDPE grade 1508S (Sinopec, China) with a weight average molecular weight of 67,849, a molecular weight distribution of 5.334 and a density 0.95 g/cm^3 in solid state, which is a fiber spinning stage polymer. Based on their chemical structures, the two samples are expected to have different pressure sensitivity of viscosity. It should be mentioned that this PMMA should be dried at 90°C for at least 5 h before the rheological testing. The non-Newtonian index n involved in eq. (3) can be measured through capillary flow by eq. (5), as shown in Table I. The temperature effect on the flow ability can be denoted from the variation of non-Newtonian index n.

$$n = \frac{d\lg \tau_w}{d\lg Q} \tag{5}$$

RESULTS AND DISCUSSION

Geometrical Dependence of Viscosity and Wall Slip

Considering the temperature effect, shear viscosity of HDPE was first measured at 190 and 260°C, as shown in Figure 1. The

Table I. The Non-Newtonian Index n of HDPE and PMMA

Temperature (°C)	$n_{\text{-HDPE}}$	$n_{\text{-PMMA}}$
190	0.42	-
210	-	0.33
255	-	0.46
260	0.82	-

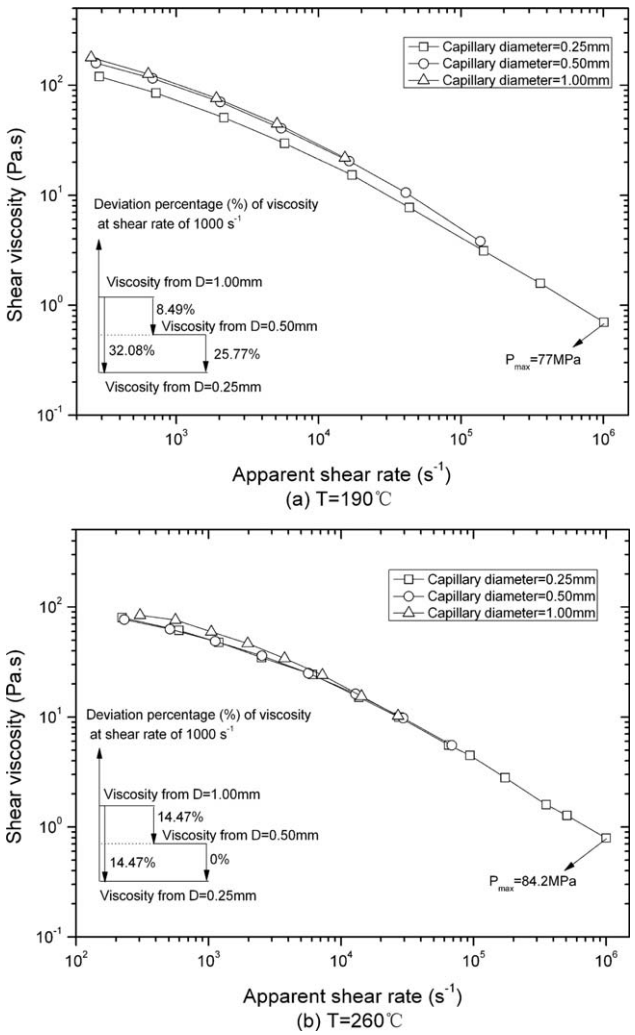

Figure 1. Shear viscosity curves of HDPE at 190 (a) and 260°C (b).

shear-heating effect during capillary flow is neglected in these capillary tests. Apart from the typical shear-thinning, geometrical dependence of shear viscosity on the die scale is observed, especially at 190°C. The shear viscosity of HDPE increases with the increase of capillary die scale within the tested range of shear rate. Similar phenomenon was widely reported by other scholars[11,12,14–16] who attributed the decrease of shear viscosity to the wall slip behavior. The deviation percentage of shear viscosity measured from the die of 0.25 mm to the die of 1.00 mm is about 32.08% under the shear rate of 1×10^3 s^{-1} at 190°C, but it decreases to 14.47% at 260°C. However, it seems that there is no deviation between the shear viscosities measured from dies of 0.25 and 0.50 mm at 260°C. In this case, slip effect can effectively explain the dependence of shear viscosity on the die scale for HDPE.[6,17–19] Similarly, shear viscosity of PMMA and deviation percentages of it between different dies at constant shear rate of 1×10^3 s^{-1} were also measured at 210 and 255°C, as shown in Figure 2. It can be found that the highest shear viscosity at 210°C is measured from the capillary die of $D = 0.25$ mm; however, at 255°C, it is from the die of 1.00 mm. Geometrical dependence of shear viscosity of PMMA at 210°C is in contrast with that at 255°C. Figure 2 shows that the shear viscosity of PMMA increases with the decrease of die diameter, but it changes totally at 255°C under which the shear viscosity decreases with the decrease of the die scale.

Generally, the slip mechanism is summarized to two modes: adsorption-desorption and entanglement-disentanglement. The essential point in figuring the slip modes is whether there is a lubricating layer between polymer bulk and wall surface during slip flow. This lubricating layer is an ultra thin melt film which is formed by entangled molecular chains. For the former slip mode, macromolecules desorbed from wall surface directly and the latter suggests disentanglement among chains happens frequently when shear stress is applied. By the way, the Mooney slip model was constructed based on the adsorption-desorption mechanism.

Here, the Mooney method, which is used to evaluate the slip velocity, is presented as

$$\frac{4Q}{\pi R^3} = \frac{4v_s}{R} + \dot{\gamma}_{true}, \tag{6}$$

where Q is volume flow rate (m^3/s), R is die radius (m), v_s is slip velocity (m/s), and $\dot{\gamma}_{true}$ is the true shear rate (s^{-1}). For a certain capillary flow, eq. (6) predicts that, for a given shear

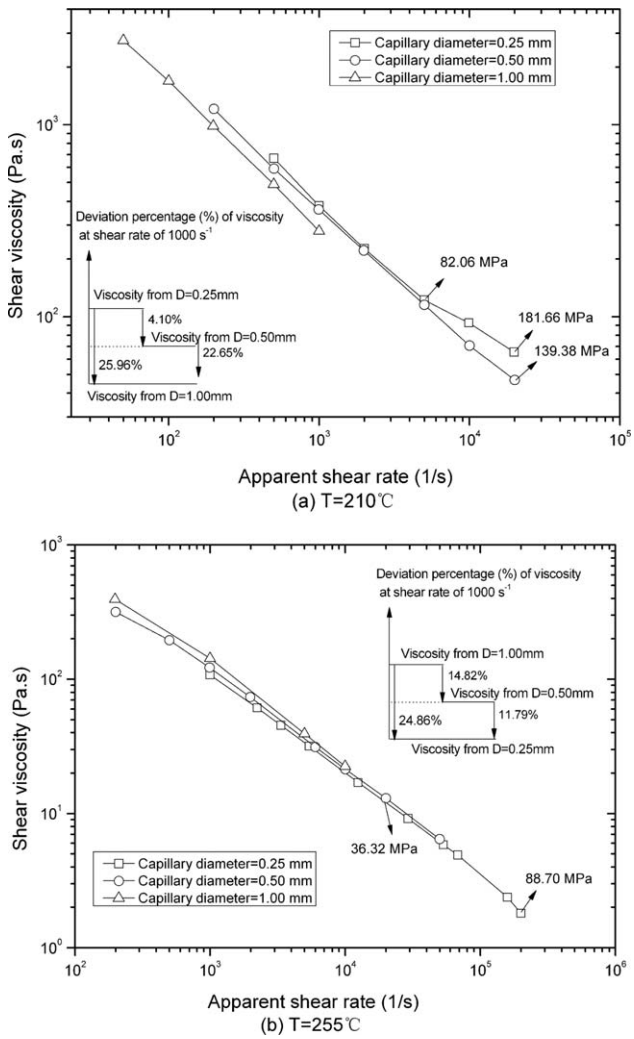

Figure 2. Shear viscosity curves of PMMA at 210 (a) and 255°C (b).

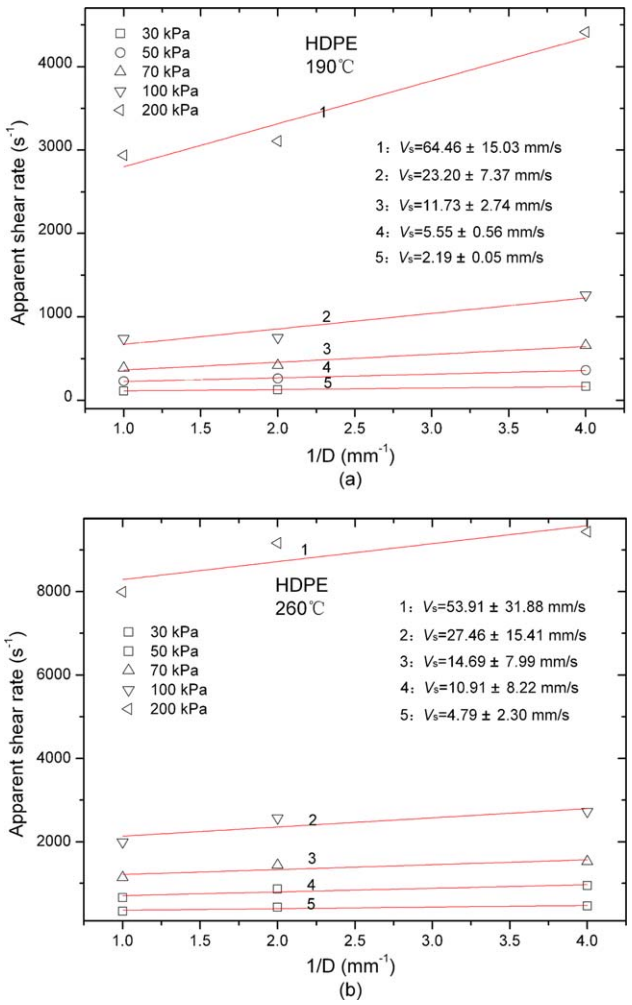

Figure 3. Analysis of slip velocity of HDPE in capillary flow at 190 (a) and 260°C (b). [Color figure can be viewed in the online issue, which is available at wileyonlinelibrary.com.]

stress, a plot of apparent wall shear rate $4Q/\pi R^3$ versus $1/R$ will has a gradient of $4v_s$ thus enabling the slip velocity to be determined.

Slip velocities v_s of HDPE and PMMA calculated under constant shear stress are shown in Figures 3 and 4, respectively. It is obviously shown that the slip velocity of HDPE largely increases with increasing the shear stress; meanwhile, increasing melt temperature also increases the slip velocity. When it comes to PMMA, however, negative slip velocity is observed at 210°C. If this is true, the PMMA melt will flow against the direction of impetus at 210°C. This is absolutely unreasonable for an absolute physical parameter. This result is similar to the Zhao's conclusion[14] which suggested that the slip mode of PMMA was entanglement-disentanglement. When the temperature increases to 255°C, however, the slip velocity becomes positive [Figure 4(b)]. Increasing temperature effectively decreases the flow resistance between molecular chains, thus leads to irregular geometrical dependence of shear viscosity. In this case, the wall slip could not be the dominant factor in determining the shear viscosity deviation any more or at least the mechanism of wall slip of PMMA in capillary flow is different from that of HDPE as reported by Zhao et al.[14]

When the shear stress overcomes the combining force of entangled molecular chains, slip happens in the lubricating layer. Figure 5 schematically shows the lubricating layer and flow velocity distribution. Disentanglement of the molecular chains between the polymer bulk and lubricating layer are expected when shear stress is applied to push melt bulk flow forward. The interaction force between the wall surface and polymer chains determines the thickness δ of the lubricating layer. If interaction between wall surface and polymer chains is weak enough and interaction among molecular chains is strong enough, the δ approaches zero and adsorption-desorption wall slip happens. In this case, flow of melt happens as whole bulk.

Pressure Sensitivity of Viscosity

In this section, pressure sensitivity of viscosity is emphasized for understanding the geometrical dependence, particularly for PMMA melt. Here, the pressure P_L which was measured from the long capillary die was adopted as the considered pressure

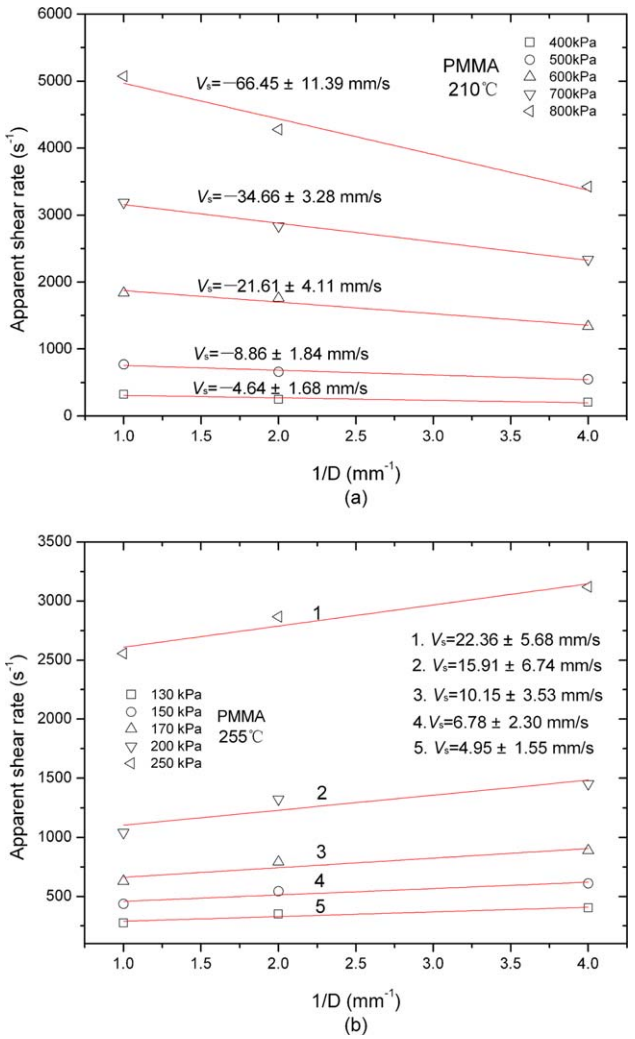

Figure 4. Analysis of slip velocity of PMMA in capillary flow at 210 (a) and 255°C (b). [Color figure can be viewed in the online issue, which is available at wileyonlinelibrary.com.]

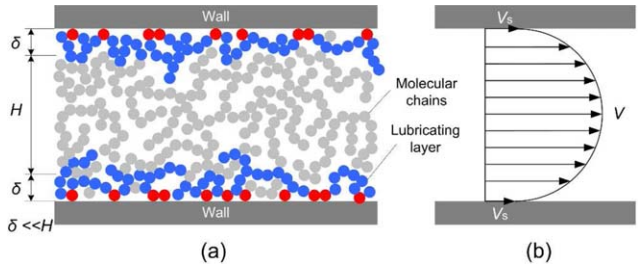

Figure 5. Schematics of lubricating layer and velocity distribution. The red dots which stick to the wall surface denote absorbed molecules in lubricating layer (blue). [Color figure can be viewed in the online issue, which is available at wileyonlinelibrary.com.]

for estimating the pressure sensitivity of viscosity. It should be noticed that the shear thinning effect of PMMA is weakened after shear rate up to 4×10^3 s^{-1} at 210°C where the melt pressure is 82.06 MPa [Figure 2(a)]. At the shear rate of 2×10^4 s^{-1}, the maximum melt pressure is up to 181.66 MPa at 210°C in the die of 0.25 mm corresponding to that of 36.32 MPa at 255°C [Figure 2(b)] under the same shear rate. Compared with the maximum pressures from the dies of 0.25 and 0.50 mm, there is a 42.28 MPa pressure difference. Significant increases of the melt pressure and less shear-thinning behavior are observed simultaneously. Such phenomenon is neither found from the results of the HDPE nor observed from PMMA when its melt temperature increases to 255°C. The maximum pressure at 255°C is only about 88.70 MPa under the shear rate of 2×10^5 s^{-1} from the die of 0.25 mm. Pressure drops between the pressure from long die and the pressure from orifice die during capillary flow of HDPE and PMMA are shown in Figure 6(a) and (b), respectively.

Similarly, pressure sensitivity of shear viscosity of HDPE is also considered even though it is not as significant as that of PMMA. Under the same shear rate of 1×10^6 s^{-1}, the melt pressures tested from the long capillary die are 77.0 MPa at 190°C and 84.2 MPa at 260°C [Figure 1(b)], respectively. Almost equal shear viscosities are obtained from three pairs of die after the shear rate of 1×10^5 s^{-1} at 260°C. This implies that HDPE melt pressure does not largely vary between 190 and 260°C as that happens to PMMA. Furthermore, the geometrical dependence of shear viscosity of HDPE nearly disappears at 260°C.

Significance of melt pressure on shear viscosity was early evaluated through the Barus equation as

$$\eta = \eta_{P_0} e^{\beta(P-P_0)}, \tag{7}$$

where η_{P0} is the viscosity (Pa s) at atmospheric pressure, β is the pressure coefficient (GPa^{-1}), P is the practical pressure (GPa) applied on the melt during flow, and P_0 is the ambient pressure (GPa). In capillary extrusion, P_0 can be treated to be zero and the viscosity η_{P0} is supposed to be constant under certain shear rate and temperature. Then, eq. (7) can be rewritten in a more useful form:

$$\ln \eta = \beta P + \ln \eta_{P_0}. \tag{8}$$

Equation (8) predicts that, for a constant shear rate or a constant shear stress, pressure coefficient β is relevant to the slope rate of the plot of logarithm shear viscosity $\ln\eta$ vs. P, thus enabling β to be determined. However, the values of β in various literatures present large variation, which was depending on the method used or the shear rate range under investigation.[31] And, it is also difficult to separate temperature, pressure, and slip effects with techniques.[39,40] Under a certain shear rate, pressure drops between long die and zero die are helpful to indirectly evaluate the pressure sensitivity of shear viscosity and to compare the effect of elevated pressure on the shear viscosity, as shown in Figure 6. Increasing melt temperature can effectively decrease the melt pressure drop under the same shear rate and then decrease the viscosity, especially for PMMA. For example, the capillary die of 0.25mm was used to measure shear viscosity and pressure drop under several discrete stages of shear rate at 210°C.[13] Actually, slip still exits for PMMA at 210°C during capillary flow, but it could not be the dominant factor affecting geometrical dependence of shear viscosity any more and could be masked by the pressure sensitivity in analyzing the slip velocity according to Mooney model.

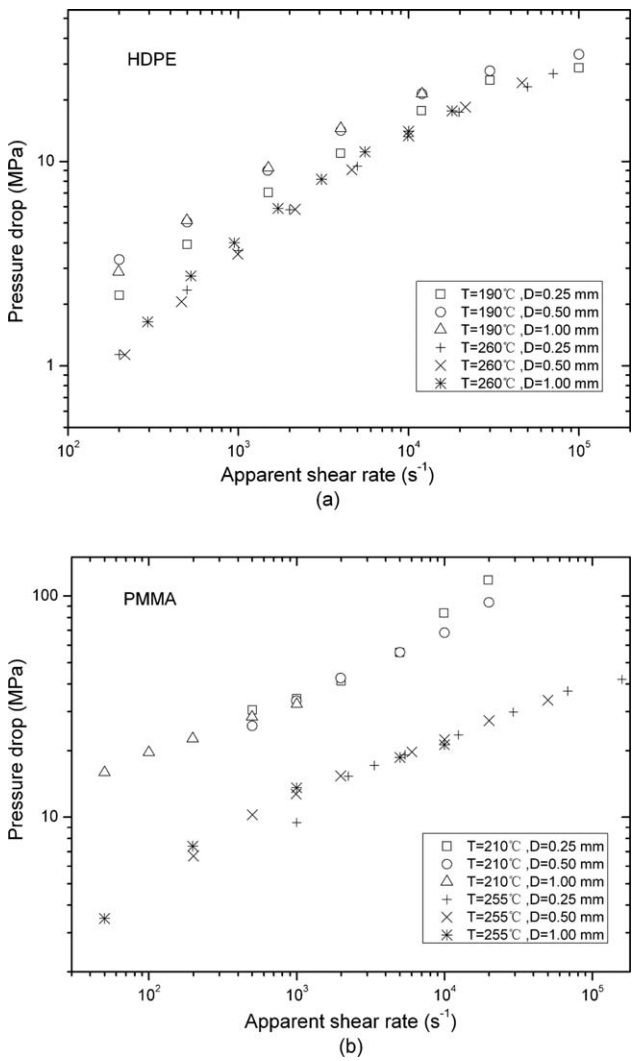

Figure 6. Pressure drops of HDPE (a) and PMMA (b) during capillary extrusion.

Table II. Overview of the Pressure Coefficients β Reported in Literatures

T (°C)	β_{HDPE} (GPa^{-1})	T (°C)	β_{PMMA} (GPa^{-1})
150	9.5[29]	210	37[31]
170	10[29]	220	25[29]
200	59[25]	220	48[25]
200	10.5[29]	240	36[30]

Pressure coefficients order the pressure sensitivity of viscosity in capillary extrusion: PMMA > HDPE, which have been well documented.[25,29] Several examples of β are summarized in Table II.

For understanding the contrary geometrical dependence of capillary viscosity of PMMA at 210°C, a shift factor a_P is defined based on the Barus effect for further estimating the pressure effect, as shown in eq. (9).

$$a_P = e^{\beta(P-P_{ref})} \tag{9}$$

where P is the practical pressure (GPa) and P_{ref} is the reference pressure (usually atmospheric pressure, i.e., $P_{ref} = 0$). To exclude the dependence of slip effect on the die diameter, viscosity curves, which were repeatedly measured from die D = 0.25 mm, are particularly considered and can then be shifted onto a set of master curves by using the appropriate shift factor a_P for each combination of pressure. During these repeated measurements, the melt inner pressure should be released fully and then the next running was restarted immediately; therefore, the PMMA bulk was compressed again and again. In this work, half value of the pressure P_L which was measured from long die was treated as the practical pressure, i.e., $P = P_L/2$. This capillary measurement was consistently conducted for eight times, as shown in Figure 7.

The shift factor can be used to calculate reference viscosity η_{ref} by dividing the measured shear viscosity by a_P, as shown in eq. (10). Here, the pressure coefficient β of PMMA is selected as 37 GPa^{-1} which obtained based on a superposition method by Cardinaels et al.[31]

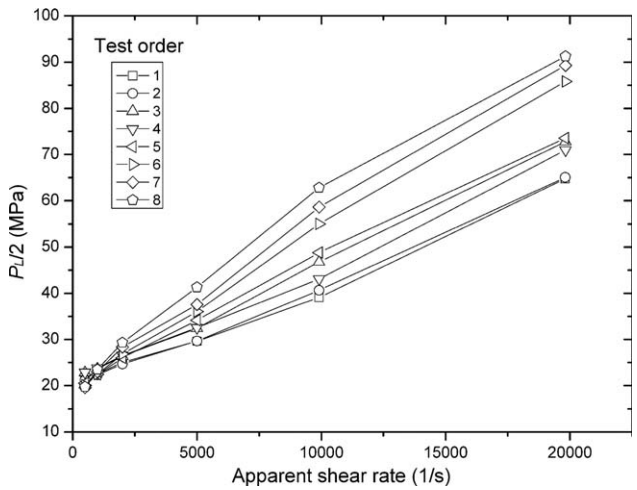

Figure 7. Practical pressures $P_L/2$.

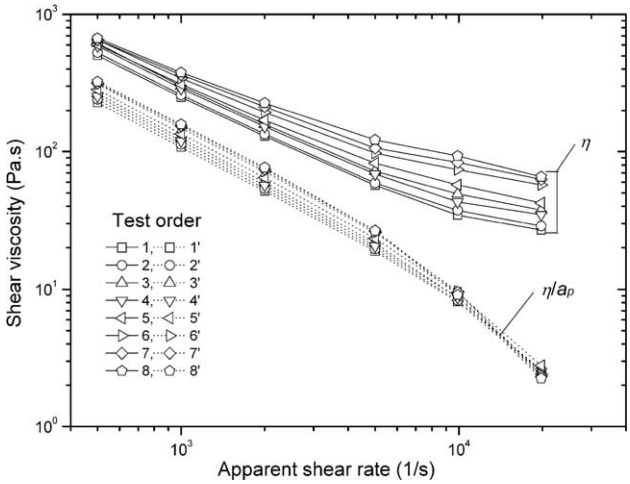

Figure 8. Corrected and uncorrected viscosity curves of PMMA measured from the die of 0.25 mm at T = 210°C.

$$\frac{\eta}{a_P} = \eta_{ref} \tag{10}$$

As shown in Figure 8, the raw viscosity data η are effectively reduced by excluding the pressure effect. Parallel plots of $\dot{\gamma}$ vs. η_{ref} are presented under lower shear rates. Although difference still can be found from the η_{ref} curves due to invisible factors, less shear-thinning behavior, which is observed from the raw viscosity curves, disappears and reference shear viscosities above 1×10^4 s^{-1} are nearly coincide. Moreover, shear viscosities shown in Figure 2(a) are also corrected with eq. (10), as shown in Figure 9. It is interesting that the shear viscosity measured from die of 0.25 mm is less than that measured from die of 0.50 mm under high shear rates. After excluding the pressure effect, "thinning" geometrical dependence of shear viscosity is observed above 2×10^3 s^{-1} at 210°C, but this can not be found under low shear rates. It seems that based on Mooney model, different slip behaviors were shown in this capillary flow for PMMA melt. Deviation between shear viscosity curves below 2×10^3 s^{-1} could be attributed to the effect of entrance. The contraction ratios ($D_{barrel}/d_{capillary}$) around entrance region are

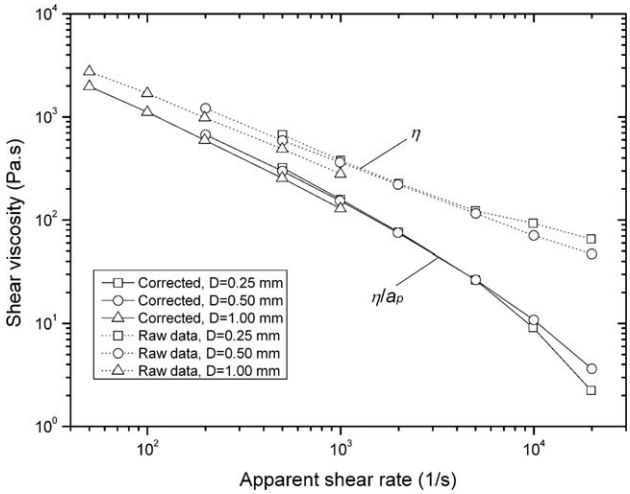

Figure 9. Comparison of geometrical dependence of viscosity of PMMA between raw data η and corrected data η/a_P

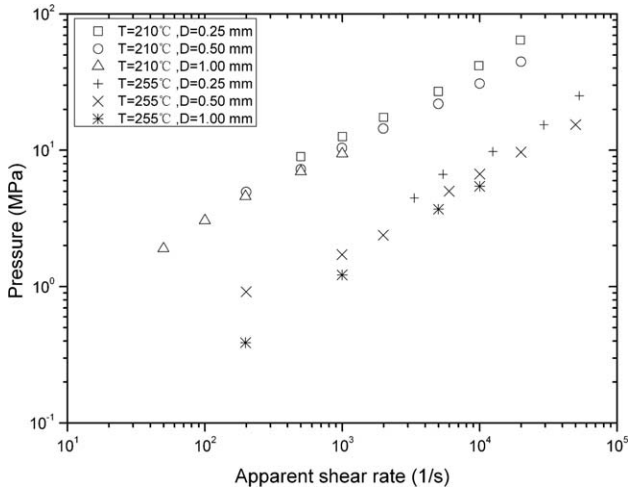

Figure 10. Comparison of pressures measured from orifice die between 210 and 255°C for PMMA.

15 ($d_{capillary}$ =1.00 mm), 30 ($d_{capillary}$ =0.50 mm), and 60 ($d_{capillary}$ =0.25 mm), respectively. Although similar pressure drops are shown in Figure 6(b) at a certain temperature, vortex behavior will be more significant in those small capillary dies. Meanwhile, it is difficult to obtain the genuine pressure value for eq. (9) in this work, and this is the very limitation by using capillary rheometer to consider pressure effect of viscosity without a pressure chamber. The open-outlet and abrupt-contraction largely affect the flow behavior of polymer melt. Figure 10 shows the pressures measured from the orifice die. There is a much more significant entrance pressure drop at 210°C; however, minor difference can be found between those measured at 210°C from different capillaries at low shear rate. It is still implied that for PMMA the pressure is almost the governed factor affecting the shear viscosity under high shear rate during capillary extrusion.

Evaluation of Free Volume and Interaction

Contribution of pressure to the viscosity is generally attributed to the dependency of free volume on pressure, which can be estimated through pressure–volume–temperature (PVT) measurement. Effect of free volume on shear viscosity was discussed by Doolittle as early as 1951.[19] The free-volume component was considered as a crucial factor and was introduced into the viscosity model as

$$\begin{aligned}\ln \eta_s &= B\left(\frac{V_0}{V_f}\right)+\ln A \\ &= B\left(\frac{1}{FFV}-1\right)+\ln A\end{aligned} \tag{11}$$

where η_s is the shear viscosity (Pa·s), A and B are constants for a single substance, FFV is the fraction of free volume (%), V_0 and V_f are the occupied volume and free volume (Å^3), respectively. Equation (11) describes the relationship between free volume and viscosity. The pressure effect on viscosity was finally considered by the effect of pressure on the FFV. Thus, viscosity can be treated as a function of temperature T, strain rate $\dot{\gamma}$ and pressure P, i. e. $\eta_s=f(\dot{\gamma}, P, T)$. In addition, the free volume dependency on viscosity was also studied by computation based on PVT behavior by Utracki and Sedlacek.[41] Simha and Somcynsky (S-S)[42–44] published a lattice–hole theory of liquids, not only describes the PVT surface, but also explicitly provides the free volume parameter as a function of temperature and pressure. Temperature sensitivity of shear viscosity of both HDPE and PMMA were estimated by Couch and Binding[29] through the term of temperature coefficient a_T based on the eq. (12) which was derived from the Arrhenius expression. This type of term can be used for describing the variation of viscosity with temperature provided the range of temperature is not very large. The temperature coefficients of HDPE and PMMA are reported to be 3600 and 12,500 ^{0}K in Couch and Binding's work (actually there is a decreasing order of $a_{T\text{-HDPE}} < a_{T\text{-PP}} < a_{T\text{-PS}} < a_{T\text{-PMMA}}$).[29] It can be seen that temperature plays different roles in the capillary viscosity between HDPE and PMMA. Because the temperature coefficient represent the significance of temperature effect on the viscosity, thus changing temperature can also in somewhat change the geometrical dependence of shear viscosity of polymer melt. The temperature coefficient can be given as

$$a_T=\frac{E}{R}\left(\frac{1}{T}-\frac{1}{T_{ref}}\right), \tag{12}$$

where E is the activation energy (kJ/mol), R is the universal gas constant, T is the practical temperature (K), and T_{ref} is the reference temperature (K).

In this section, effect of free volume on capillary viscosity was investigated through molecular dynamics simulation (MDS) under static state, which was further employed to estimate the interaction between intermolecular chains. COMPASS (condensed-phase optimized molecular potentials for atomistic simulation studies) force field, which can be used for the condensate and Vdw non-bond energy, and Number-Pressure-Temperature (NPT) assembling system are preferred to consider the periodic boundary unit. Constant amount of atoms were assumed to be gathered within this periodic unit. If one atom escapes from this unit, there will be another identical atom comes into at the same time. Although the chain morphology in the bulk is different from that near the wall surface, this is nonrelated to this interaction calculation which focuses on the movements of atoms. The Lenard-Jones (L-J) potential function is adopted in the calculation of Vander Waals (Vdw) interaction, which is shown in Figure 11, in which $E(r)$ is potential energy, $r(\sigma)$ is the distance which presents a threshold value of r_0. When the distance of separation is less than r_0, the repulsive force will take place. When the distance of separation is larger that r_0, the attracting response will emerge. Here, the L-J function can be given by eq. (13). Due to its computational simplicity, the Lennard-Jones potential is used extensively in computer simulations.

$$E(r)=4\varepsilon\left[\left(\frac{\sigma}{r}\right)^{12}-\left(\frac{\sigma}{r}\right)^{6}\right] \tag{13}$$

where ε is the well depth in Figure 11 which is a measure of how strongly the two atoms attract each other, σ is the distance at which the intermolecular potential between the two atoms is zero (i.e., hard sphere diameter), and r is the distance between two atoms.

Movements of atoms are considered in the other atoms and the interaction force between these atoms is calculated. The energy function used in COMPASS force field is shown in eq. (14) as following.

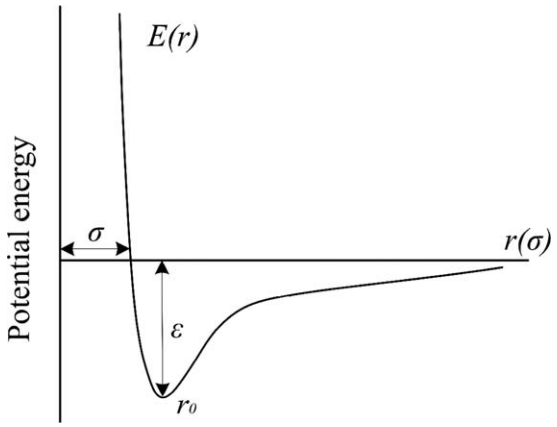

Figure 11. Lenard-Jones potential function.

$$E_{ij}=\sum_{i,j}\varepsilon_{ij}\left[2\left(\frac{r_{ij}^0}{r_{ij}}\right)^9-3\left(\frac{r_{ij}^0}{r_{ij}}\right)^6\right] \quad (14)$$

where E is potential energy, i is the charge acceptor, j is the charge donator, ε is the dielectric constant, r_{ij} is atom distance, and r_{ij}^0 is the initial distance value.

Functions of temperature-control and pressure-control are selected as the Andersen method and the Berendsen method, respectively. And energy of interaction such as Vdw interaction and electrostatic interaction are given by L-J function and Coulomb function, respectively.[14,44] The simulation time is 100 ps and the step number is set at 10^5. Total energy E_{total} can be given as the sum of the corresponding energy as

$$E_{total}=\left(E_b+E_\theta+E_\phi+E_\omega+E_c\right)+\left(E_h+E_e+E_v\right), \quad (15)$$

where E_b is bond energy, E_θ is angle energy, E_φ is torsion energy, E_ω is out-of-plane energy, E_c is cross interaction energy, E_h is hydrogen-bond interaction, E_e is electrostatic interaction energy, and E_v is Vdw interaction energy. Although the MDS is carried out in equilibrium state and the pressure sensitivity of viscosity during capillary flow is detected in a fast flow state under which the polymer chains were highly orientated and stretched, the simulated FFV and the interaction on the microscopic scale are still effective for considering the bulk and interface effect.

PMMA amorphous construction model with two molecular chains which contain 100 repeat units of ($C_5H_8O_2$) and HDPE amorphous construction model with two molecular chains which include 200 repeat units of (C_2H_4) are built, as shown in Figure 12. The red atom is oxygen (O), the black atom is carbon (C), and the gray atom is hydrogen (H). Temperatures for PMMA are set at 210, 225, 240, and 255°C, and temperatures for HDPE are set at 155, 190, 225, and 260°C, respectively. Pressure range is set at 10–250 MPa with a constant span of 50 MPa.

The compressibility of PMMA and HDPE melts is first studied, as shown in Figure 13. Although it seems there is a stronger pressure dependency of viscosity for PMMA at 255°C, the absolute value of FFV under 175 MPa and 255°C is almost equal to that under 10 MPa and 210°C. It should be noticed that a higher FFV is helpful to reduce the essential pressure (Figure 10) which is required to push the melt flow forward. Increasing temperature can effectively decrease entrance pressure during capillary flow. Thus, large increase of pressure can be hardly found at the same shear rate under high temperature.

If the FFV curve of PMMA at 210°C [Figure 13(a)] can be shifted onto the one under 255°C while keeping its y-axis value unchanged (i.e., temperature-independent transition), the pressure dependency of viscosity under 210°C and 10 MPa will be identical with that under 255°C and 175 MPa according to the Doolitte equation. Nevertheless, the maximum pressure under 255°C measured from the long capillary die is only about 88.7 MPa, which is far lower than that of 175 MPa. The pressure effect apparently leads to the dissimilar geometrical-dependence of PMMA at 210 and 255°C. However, similar result can not be observed in Figure 13(b) in which FFV of HDPE between

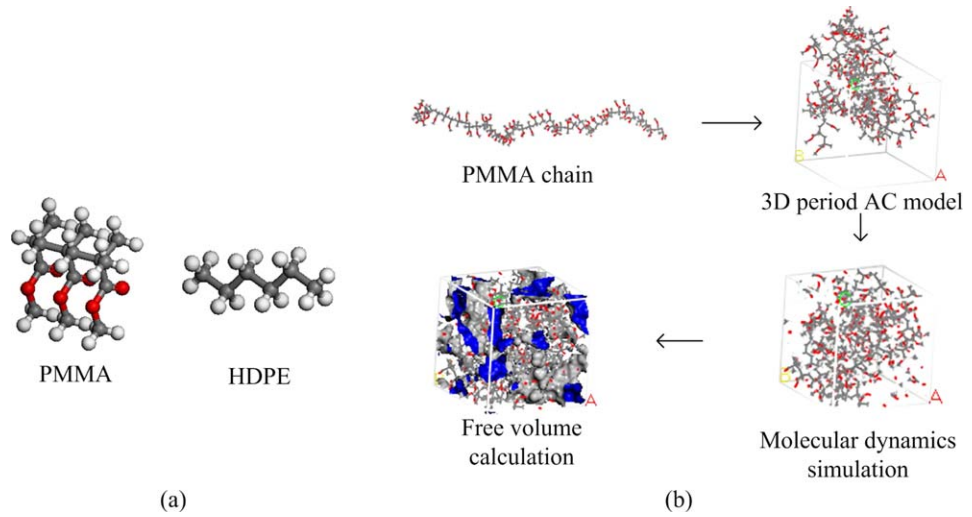

Figure 12. Repeat units of PMMA and HDPE (a) and MDS process of PMMA (b). [Color figure can be viewed in the online issue, which is available at wileyonlinelibrary.com.]

different temperatures presents smaller difference than that of PMMA. The FFV value of HDPE under 190°C and 10 MPa is almost equal to that under 260°C and 100 MPa, but the difference of FFV between 10 and 100 MPa is less that 2% at both 190 and 260°C.

In addition, interaction energy of both polymers is deliberately investigated for considering the combining strength between molecules. The total energy mainly includes potential energy and kinetic energy, and potential energy contains Vdw interaction and electrostatic interaction. As the different molecular polarity, the dominant energies for PMMA and HDPE are the potential energy and the kinetic energy, respectively. The Vdw dispersive energy and the electronic energy have an attracting function which can enhance the combinations of molecular chains, and the Vdw repulsive energy has an excluding function. Thus, the attracting force (electronic and dispersive) to the excluding force (repulsive) ratio, which represents the proportion of these two functional forces, is defined as λ to quantify the combining strength among molecular chains, as shown in eq. (16).

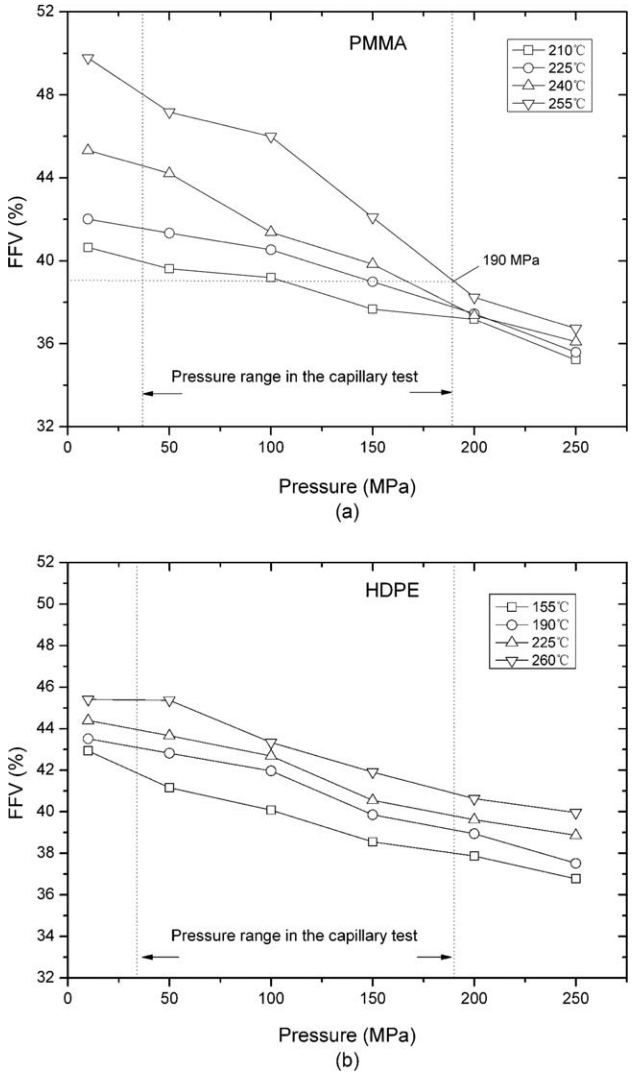

Figure 13. FFV of PMMA (a) and HDPE (b) from Material Studio.

Table III. Interaction Parameters

Parameters	PMMA	HDPE
λ	1.40	1.13
r[14]	1.77	1.62
CED (MJ/m^3)	347	259

$$\lambda = \frac{|E_{dis}| + |E_e|}{|E_{rep}|}, \quad (16)$$

where E_{dis} is the Vdw dispersive energy (kcal/mol), E_{rep} is the Vdw repulsive energy (kcal/mol) and E_e is the electronic energy (kcal/mol). Except for the interaction ratio, cohesive energy density (*CED*), which also represents the intimate combining strength among molecular chains, reflects that there is a stronger combining strength for PMMA molecules causing a higher flow resistance during disentanglement-flow. Although the *CED* was found to be the dominant factor affecting the polymer–polymer sliding friction in solid state,[45] the viscosity implying the interfriction among molecular chains is also affected by *CED*.[46,47] In addition, combining strength between molecular chains and Fe atoms of wall surface was also reported by Zhao et al.[14] Three interaction parameters are summarized in Table III.

As shown from the MDS results, no dependence of λ on the melt temperature or the pressure is observed. It is found from Table III that stronger combining strength between the molecular chains of PMMA is observed than that of HDPE. The ratio of attracting force to excluding force between the interface of melt and wall surface was defined as r in Zhao's conclusion.[14] For PMMA, not only the interaction among molecular chains but also the interaction between chains and the Fe atom of surface wall is stronger than that of HDPE. The occurrence of cohesive slip is highly dependent on the interaction between the polymer and the wall, whereas the disentanglement slip is related to the interaction among molecular chains. This implies again that the irregular geometrical dependence of PMMA viscosity can not be attributed to the wall slip behavior. Meanwhile, it can be seen from Figure 2 that higher temperature effect on viscosity is presented for PMMA. Thus, increasing temperature leads to the different viscosity behavior for PMMA at 210 and 255°C, but similar viscosity behavior is observed for HDPE at 190 and 260°C.

CONCLUSIONS

The geometrical dependence of viscosity of polymer melts could be affected by multiple factors, such as wall slip, pressure, and temperature. This work focused on exploring the mechanism of geometrical dependence of shear viscosity of PMMA and HDPE. Experimental results showed that the shear viscosity of PMMA increased with the decrease of the die scale at 210°C, but it was quite opposite at 255°C; however, shear viscosity of HDPE decreased with the increase of the die scale at both 190 and 260°C. Significant pressure difference between capillary die and orifice die was shown for PMMA between 210 and 255°C, which could not be found for HDPE between 190 and 260°C. In addition, the capillary viscosity of PMMA measured with the die of D = 0.25 mm at 210°C became less thinning when the

melt pressure was up to 181.66 MPa. It was found that the negative slip velocity obtained from Mooney method was hardly effective to explain the geometrical dependence of shear viscosity for PMMA at 210°C, which was further attributed to the pressure sensitivity of viscosity. Based on a shift factor a_P derived from the Barus equation, capillary viscosity curves of PMMA measured under different pressures could be shifted on to a set of parallel plots after correcting the pressure effect and then less shear-thinning disappears, especially at high pressure. Moreover, the FFV of PMMA melt presented a higher dependence on melt temperature and pressure, which resulted in an irregular pressure sensitivity of viscosity according to the Doolittle model. Higher combining strength ratios of λ among molecular chains and of r between molecular chains and Fe atoms of wall surface as well as higher *CED* were also found for PMMA than those of HDPE. This indicated that combining strength of the PMMA molecular chains was formed more tightly, which further caused higher pressure sensitivity of viscosity under the same pressure. In brief, it could be concluded that the geometrical dependence of capillary viscosity of PMMA was largely attributed to the pressure sensitivity of viscosity, which was dependent on the effects of free volume and interactions.

REFERENCES

1. Tsai, M. H.; Ou, K. L.; Huang, C. F.; Cheng, H. C.; Shen, Y. K.; Chang, C. Y.; Wu, C. H.; Chen, J. H.; Guan, P. *J. Int. Commun. Heat Mass. Transfer.* **2008**, *35*, 1097.
2. Song, M. C.; Liu, Z.; Wang, M. J.; Yu, T. M.; Zhao, D. Y. *J. Mater. Process Technol.* **2007**, *187*, 668.
3. Sha, B.; Dimov, S.; Griffiths, C.; Packianather, M. S. *J. Mater. Process Technol.* **2007**, *183*, 284.
4. Ou, J.; Perot, B.; Rothstein, J. P. *Phys. Fluids.* **2004**, *16*, 4635.
5. Zhang, N.; Gilchrist, M. D. *Polym. Test.* **2012**, *31*, 748.
6. Chen, S. C.; Tsai, R. I.; Chien, R. D.; Lin, T. K. *Int. Commun. Heat Mass. Transfer.* **2005**, *32*, 501.
7. Komuro, R.; Kobayashi, K.; Taniguchi, T.; Sugimoto, M.; Koyama, K. *Polymer* **2010**, *51*, 2221.
8. Chien, R. D. *Sens. Actuator. A-Phys.* **2006**, *128*, 238.
9. Chen, C. S.; Chen, S. C.; Liao, W. H.; Chien, R. D.; Lin, S. H. *Int. Commun. Heat Mass Transfer.* **2010**, *37*, 1290.
10. Chen, S. C.; Liao, W. H.; Yeh, J. P.; Chien, R. D. *Polym. Test.* **2012**, *31*, 864.
11. Chien, R. D.; Jong, W. R.; Chen, S. C. *J. Micromech. Microeng.* **2005**, *15*, 1389.
12. Chen, C. S.; Chen, S. C.; Liaw, L. W.; Chien, R. D. *Eur. Polym. J.* **2008**, *43*, 1891.
13. Lin, X.; Kelly, A.; Ren, D. Y.; Woodhead, M.; Coates, P.; Wang K. S. *J. Appl. Polym. Sci.* **2013**, *130*, 3384.
14. Zhao, D.; Jin, Y.; Wang, M.; Song, M. *J. Mech. Eng. Sci.* **2010**, *225*, 1175.
15. Zhao, D.; Jin, Y.; Wang, M. *Polym. Eng. Sci.* **2012**, *52*, 1806.
16. Münstedt, A. H.; Schmidt, M.; Wassner, E. J. *J. Rheol.* **2000**, *44*, 413.
17. Hatzikiriakos, S. G.; Dealy, J. M. *J. Rheol.* **1992**, *36*, 845.
18. Münstedt, H.; Schmidt, M.; Wassner, E. *J. Rheol.* **2000**, *44*, 413.
19. Ansari, M.; Hatzikiriakos, S. G.; Mitsoulis, E. *J. Non-Newtonian Fluid Mech.* **2012**, *167*, 18.
20. Doolittle, A. K. *J. Appl. Phys.* **1951**, *22*, 1471.
21. Christmann, L.; Weber, G. *Rheol. Acta.* **1978**, *17*, 16.
22. Kelly, A. L.; Gough, T.; Whiteside, B. R.; Coates, P. D. *J. Appl. Polym. Sci.* **2009**, *114*, 864.
23. Rides, M.; Kelly, A. L.; Allen, C. R. G. *Polym. Test.* **2011**, *30*, 916.
24. Kelly, A. L.; Krajnc, M. *Polym. Eng. Sci.* **2008**, *48*, 1815.
25. Binding, D. M.; Couch, M. A.; Walters, K. *J. Non-Newtonian Fluid Mech.* **1998**, *79*, 137.
26. Cidade, M. T.; Fernandez, M.; Filipe, S.; Santamaria, A. *Polym. Test.* **2012**, *31*, 290.
27. Son, Y. *J. Polym. Res.* **2009**, *16*, 667.
28. Maxwell, B.; Jung, A. *Mod. Plast.* **1957**, *35*, 174.
29. Couch, M. A.; Binding, D. M. *Polymer* **2000**, *41*, 6323.
30. Fernádez, M.; Muñoz, M. E.; Santamaría, A.; Sysjälä, S.; Aho, J. *Polym. Test.* **2009**, *28*, 109.
31. Cardinaels, R.; Puyvelde, P. V.; Moldenaers, P. *Rheol. Acta.* **2007**, *46*, 495.
32. Liang, J. Z. *Polymer* **2001**, *42*, 3709.
33. Barus, C. *J. Proc. Am. Acad.* **1981**, *27*, 13.
34. Koran, F.; Dealy, J. M. *J. Rheol.* **1999**, *43*, 1279.
35. Sedlacek, T.; Zatloukal, M.; Filio, P.; Boldizar, A.; Saha, P. *Polym. Eng. Sci.* **2004**, *44*, 1328.
36. O'Connor, K. M.; Scholsky, K. M. *Polymer* **1989**, *30*, 461.
37. Alexander, Y. M.; Avraam, II. Rheology. Concepts, Methods, and Applications, 2nd ed.; ChemTec Publishing: Toronto, **2012**; pp 257–269.
38. Gebhard, S. A Practical Approach to Rheology and Rheometry, 2nd ed.; Gebrueder HAAKE GmbH: Karlsruhe, **2000**; pp 70–81.
39. Goubert, A.; Vermant, J.; Moldenaers, P.; Göttfert, A.; Ernst, B. *Appl. Rheol.* **2001**, *11*, 26.
40. Laun, H. M. *Rheol. Acta.* **2003**, *42*, 295.
41. Utracki, L. A.; Sedlacek, T. *Rheol. Acta.* **2007**, *46*, 479.
42. Simha, R.; Somcynsky, T. *Macromolecules* **1969**, *2*, 342.
43. Somcynsky, T.; Simha, R. *J. Appl. Phys.* **1971**, *42*, 4545.
44. Jaramillo, E.; Wilson, N.; Christensen, S.; Gosse, J.; Strachan, A. *Phys. Rev. B.* **2012**, *85*, 1.
45. Jia, B. B.; Liu, X. J.; Cong, P. H.; Li, T. S. *Wear* **2008**, *264*, 685.
46. Mangarj, D.; Bhatnagar, S. K.; Rath, S. B. *Macromol. Chem. Phys.* **1963**, *67*, 75.
47. Bristow, G. M.; Watson, W. F. *Trans. Faraday Soc.* **1958**, *54*, 1742.